DEVELOPMENT AND TESTING OF A NEW HIGH FLOW CENTRIFUGAL PIPELINE BOOSTER

by

Robert H. Meier
Chief Designer
and
Robert N. Schiller
Design Engineer
Centrifugal Compressors
Cooper Energy Services
Mount Vernon, Ohio

Robert H. Meier is in charge of Design and Development of Centrifugal Compressors at Cooper Energy Services.

Born and educated in Switzerland, (Officers Candidate School, 1962, and Federal Institute of Technology: Mechanical Engineering, 1966), Mr. Meier immigrated to the U.S.A. to join Cooper Energy Services in 1966. Following a brief training program, he started to work in his present field, designing centrifugal compressors for widely varying applications and conditions. Later development and performance testing and analysis were added to his responsibilities.

Robert N. Schiller has been an engineer with Cooper Energy Services four years. He has spent three years in Centrifugal Design and is currently in Rotating Product Marketing as a sales engineer.

He received a B.S. (Mechanical Engineering) degree from the University of Southwestern Louisiana in 1972 and an M.S. degree (Gas Turbine Laboratories, Mechanical Engineering Department) from Texas A&M University in 1973.

He is a member of the A.S.M.E., several honorary societies, and a certified emergency medical technician.

ABSTRACT

Development of a high-flow gas transmission compressor designed for maximum efficiency and servicing ease is presented. Design techniques involving the use of a finite element stress computer program and elemental impeller blade loading are discussed. Corroborating stress/strain data established from casing model and full size hydrostatic testing are included.

A tabulation of performance results derived from moderate and low pressure closed loop testing, including the effects of guide vane positioning, are of special importance. A brief review of materials selection for high strength at low temperatures and some thrust bearing test data is also of some interest.

INTRODUCTION

In the development of a new pipeline centrifugal compressor, several new techniques were applied, and results from both analytical and test studies are of general engineering interest.

Major emphasis was placed on aerodynamic performance and casing stress and deflection. These areas were felt to be of major importance to future industry needs. The criteria selected for the design was based on a survey of potential future requirements, mainly for arctic environments. The main points were:

(1) Maximum efficiency

(2) Relatively high flow (15 - 30,000 ACFM)

(3) High pressure level (1400 - 1800 psig)

(4) Low temperature exposure (−100°F ambient, −20°F gas)

(5) Reliability and low maintenance requirements

(6) Moderate pressure ratio (1.1 - 1.3)

DESIGN CONCEPT

The analysis of the main design criteria led to the definition of a 36-inch, single-stage design to best satisfy the high flow and low head requirements. Pressure rating and suitability for low temperature exposure and operation were factors primarily affecting casing design and material selection. This left the need for maximum efficiency as the only main criterion yet to be considered. Further studies confirmed that it was this requirement for top aerodynamic efficiency which required the most concerted design and development effort to produce the necessary improvements, possibly resulting in a radical departure from well-established centrifugal pipeline booster designs.

Aerodynamic Design

To pinpoint the areas with potential for efficiency improvements, and to determine the possible quantitative effects of such improvements, three separate investigations were carried out:

1) An analytical evaluation of all major loss-areas in pipeline boosters.

2) Experimental evaluation of high-flow impeller designs using a conventional 14-inch booster as test vehicle.

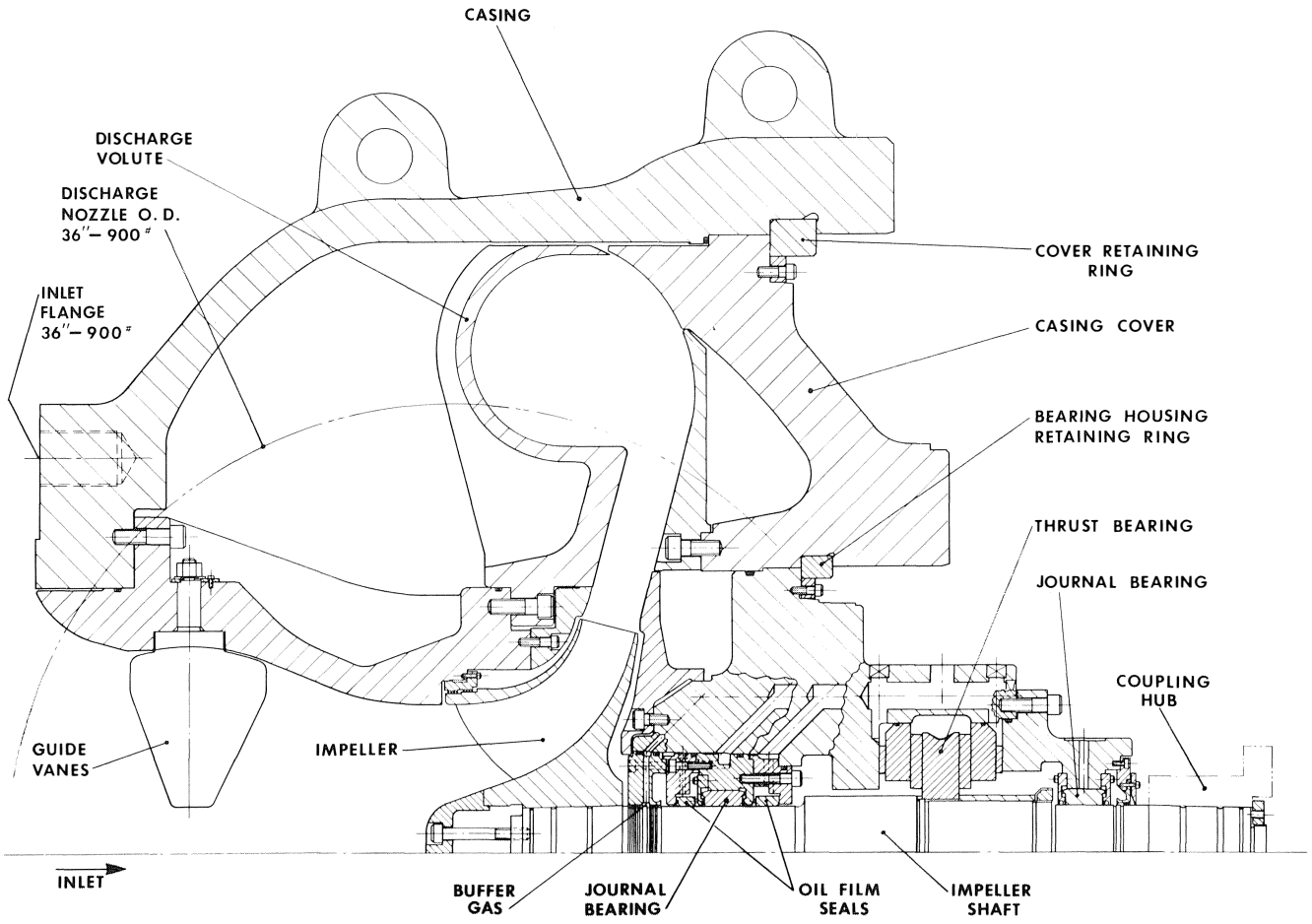

Figure 1. Cross Section of Compressor.

3) Review of past experience with the design, production and performance testing of high-flow aerodynamic assemblies for traditional booster configurations.

These investigations clearly identified the adoption of an axial inlet, greatly increased precision in the production of fully fabricated impellers and substantial improvements in area and surface control in all gas passages as the areas with greatest potential for significant overall performance improvement.

In addition, it was concluded that, through reasonable advances in design and production techniques in these areas, an overall aerodynamic booster efficiency of 85 - 87% (isentropic) should be realized.

The actual work to develop the production techniques necessary to achieve the required high precision began in 1972 and extended into 1974. The bulk of the effort went into the development of greatly improved impeller blade contour control, inspection tooling, blade positioning and holding, the definition of welding parameters minimizing distortion, and impeller assembly inspection tooling techniques.

The direct influence of the conclusions from the different investigations on the final general aerodynamic design can be clearly seen in Figures 1 and 2; the axial inlet represents the most apparent departure from traditional designs.

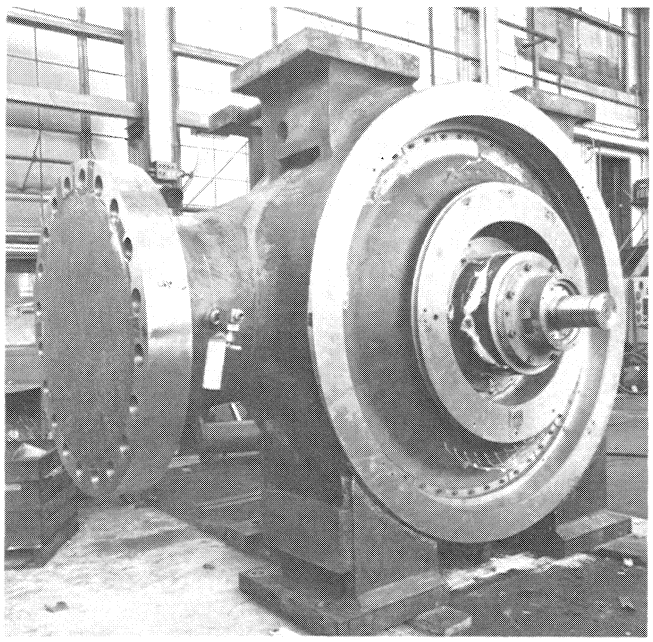

Figure 2. Prototype, Fully Assembled.

The completely fabricated impeller, shown in Figure 3, is fully shrouded and of a mixed-flow design; a configuration imposed by primarily geometric considerations resulting from the high flow/low head requirement.

The blade consists of a long, modestly loaded inducer section followed by a backward swept exit to provide the typically preferred wide operating characteristic.

Casing Design and Material Choice

The final casing configuration, shown in Figures 1 and 2, is the result of an extensive development effort over an active period of about two years. In addition to configuration changes, the design requirements for this casing were revised from an originally fully fabricated construction, capable of pressure levels up to 1500 PSIG, to a cast casing rated at 1800 PSIG maximum working pressure. These revisions were necessitated by changes in emphasis of installation and operating requirements and economic realities. Major phases of this analytical and experimental work are covered in a subsequent section.

From the very beginning, in the conceptual phase of the casing design, the requirement for a rugged construction with maintenance ease demanded special attention. Problems in this area are primarily caused by the large physical size imposed by the high flow requirements and the relatively high operating pressure levels. These concerns heavily influenced the final selection of a highly spherical casing design and a high-strength material.

For the original fabricated version, a medium alloy, high-strength steel known as HY-80 Modified with excellent welding qualities was chosen. This material contains around 2% Ni and 2% Cr and is used in submarine-hull construction. It was used for our ¼ scale model casing, which served as the basic vehicle for much of the casing development work and which will be subsequently discussed. Problems encountered during the initial model stress-test work required strengthening of certain highly stressed areas of casing and cover and raised concerns with the ability of plate suppliers to maintain the required material properties in increasingly heavy cross sections. With these facts, plus substantial cost escalations of plate material, the search for an alternate casing material began to concentrate on a cast solution. Ultimately, the cast casing was selected on the basis of reliability and general ruggedness.

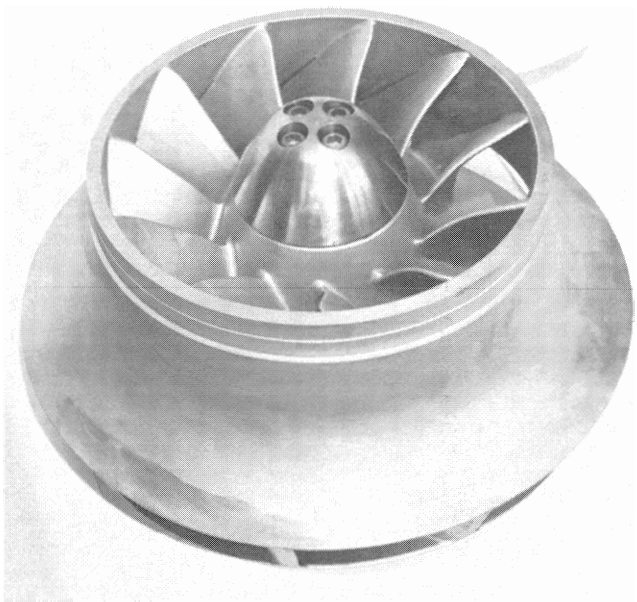

Figure 3. Prototype Impeller with Nose Piece.

The casing material selected was found in the family of 13% chromium cast steels. It was developed by George Fischer Ltd. of Switzerland. Its unique combination of high-strength, resistance to corrosion, erosion and cavitation has made it very popular in the field of European water turbine construction. These characteristics, including high fatigue strength and resistance to brittle fracture, make it particularly suitable for this application. The material designation is ASTM A-296 GR CA-6NM. In addition to the listed qualities, this material has excellent castability and low temperature properties. Also, due to its high alloy content of 13% Cr and 4% Ni, it can be quenched-out in heavy sections (of 7 to 8 inches) without loss of its high mechanical properties.

Tensile strength	110 KSI min.
Yield strength (2% offset)	80 KSI min.
Impact Charpy 'V' at −100°F	20 ft. lbs. (min.)
Modulus	$26.2 \cdot 10^6$ psi
Elongation (4D)	15%
Reduction in area	35%
Hardness	285 HB (max.)
Nil duct. temperature	−250°F

These properties confirm this material to be highly suitable for this compressor casing, particularly considering the likely low temperature exposure and operating requirements of −100°F ambient and −20°F gas temperature, respectively.

This material was used for the full-size prototype casing. No significant problems were encountered during its production. Very extensive inspection and test requirements, including full radiographic and ultrasonic inspection of all highly stressed areas, confirmed the casting approach and material selection. The absence of major problems, in spite of the large size of the casing, is mainly attributed to the close cooperation between the manufacturer and its supplier.

Overall Design

The final overall compressor design, as shown on Figure 1, admits the gas through an axial inlet to a mixed-flow impeller (prototype condition imposed), followed by a vaneless diffuser and finally through a continuous scroll-type volute into a tangential discharge nozzle.

The strongly spherically-shaped, integrally-cast casing is rated at 1800 PSIG maximum working pressure at temperatures down to −100°F. The two flanges are designed to meet a 36-inch 900 PSI ASA rating.

To accommodate the axial inlet, the rotor is of an overhung design, a well-proven arrangement frequently preferred for ease of maintenance.

Also, as a result of the axial inlet, the entire compressor is designed to be serviced from its drive-end side. To further simplify maintenance, the complete rotating assembly is removed without disturbing the main casing cover and is bench-assembled into the stationary bearing and seal assembly, as shown by Figure 4.

The retention of the main casing cover and the large bearing housing is accomplished through segmented shear rings, (Figures 1 and 2). For large diameters and higher working pressures, shear ring closures are a better design solution than the

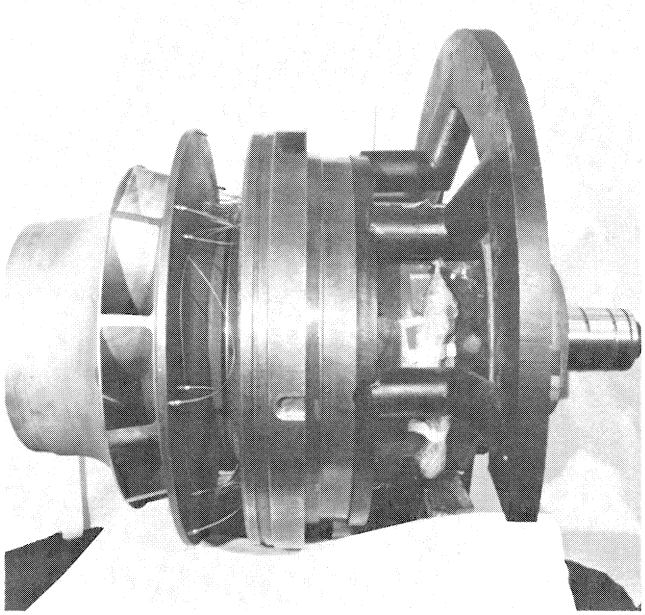

Figure 4. Rotating Element, Fully Assembled in Bearing Housing with Special Lifting Tool.

typical bolted construction. In addition, maintenance aspects are improved.

Since overhung compressor designs require generally large thrust bearings to absorb the very high thrust loads encountered during fully pressurized start-ups (up to 45,000 lbs. thrust in this case), solutions were sought to reduce the high parasitic losses associated with conventional thrust bearing designs where the rotating thrust collar revolves in a completely oil-filled housing. A newer type thrust bearing design with each thrust bearing pad individually supplied with fresh oil was investigated by CES. Figure 5 shows this bearing.

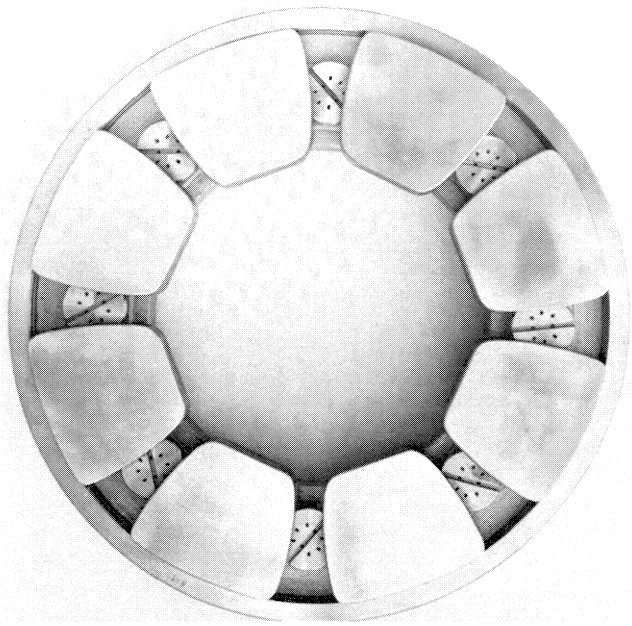

Figure 5. Direct Lube Thrust Bearing.

Less oil is required to obtain the same operating temperature and the proper operation of such thrust bearings requires a fully-drained housing. Both of these features are designed to drastically reduce bearing pad and oil temperatures by preventing excessive oil recirculation and churning. Consequently, directed-lubrication thrust bearings will produce lower parasitic HP requirements.

Figure 1 shows the use of conventional oil film, bushing-type seals to contain the pressurized gas. However, to prevent any oil from entering the aerodynamic assembly of the compressor, where it would cause substantial fouling leading to drastically reduced aerodynamic efficiencies, a buffer gas port has been provided between the impeller and the seal assembly. It is expected that the use of this buffer-port can be limited to the period before start-up and after shutdown, as during normal operation the pressure rise across the impeller maintains a positive differential across this buffer labyrinth.

Like many of its predecessors, this new pipeline booster is designed to be direct-driven by gas turbines in the medium to high power range with an operating speed range from 2500 to 5500 RPM.

CASING DEVELOPMENT

In this phase of the overall compressor development program, the casing design was subjected to two main experimental test series, both accompanied by detailed computerized Finite Element Stress Analyses to refine the casing design and confirm its suitability as a pressure vessel prior to its commitment to production.

Model Tests

Following the completion of the conceptual design, a ¼ scale model casing was fabricated from modified HY-80 material. This was done to simulate the fabricated casing originally planned.

Figure 6 shows the model casing on hydrostatic test.

In an extended series of hydrostatic pressure tests, all significant stresses and deflections were measured, recorded and critically analyzed to uncover all marginal areas for further strengthening and refinement.

Each model configuration was generously instrumented with strain gauges and dial indicators in all expected areas of

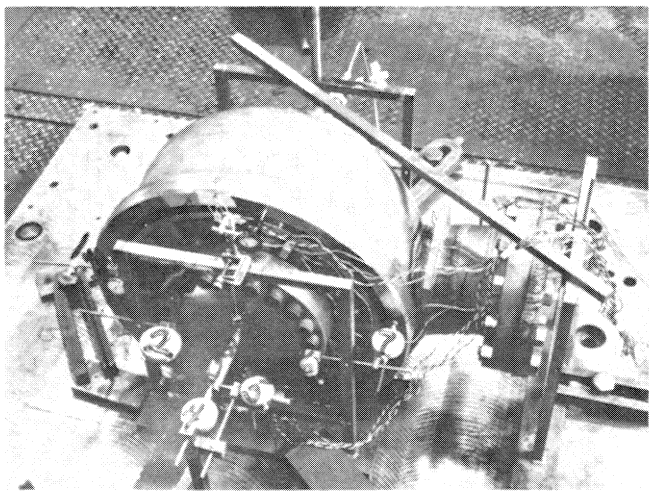

Figure 6. Model Casing in Hydrostatic Evaluation.

high stresses or deflections; in other areas where high stresses could be suspected but not precisely pinpointed, photo-elastic coatings were applied whose colour intensities and changes were closely monitored using a reflection polariscope.

The first pressure tests confirmed major problems in the vicinity of the two shear rings and the main casing cover. During these first pressure tests, the model casing exhibited .028″ axial deflection at the center of the end cover at only 400 PSIG internal pressure and the end cover itself suffered permanent deformation starting at only 200 PSIG. This was a discouraging result considering that the 1800 PSIG maximum working pressure goal required hydrostatic pressure testing at 2700 PSIG.

To permit the achievement of higher pressure levels, two different versions of reinforcing rings were successively attached to the outer casing flange to control the rolling or tipping of this area. The first of these two stiffening collars is clearly visible on Figure 7.

While these modifications permitted to reach 1800 PSIG, end cover deflections still rose to .078″ on the model. In addition, local stresses in the outer shear ring groove caused yielding near 1000 PSIG, although a redistribution of stresses sufficient to prevent fracture occurred. Stress levels elsewhere on the casing were low, except in the vicinity of the discharge nozzle-to-casing weld-joint where a maximum of 79 KSI was recorded at 1800 PSIG. The photo-elastic coating proved most useful in pinpointing peak stress areas. Stresses on the casing cover were clearly excessive throughout, at 1800 PSIG, with a maximum in the inner shear ring groove of 80 KSI.

As a result of these first tests, the casing was redesigned replacing the troublesome outer flange section with a much larger one. The end cover was replaced completely with an externally ribbed construction further supported by a bolted-on inner cover simulating the bearing housing. Although this inner cover remained fairly rigid (only .018″ radial deflection), the main cover design still proved to be inadequate, due to a deflection of the inner edges of the ribs and excessive rolling of the shear ring, leading to permanent deformation at 1600 PSIA. In addition, the stresses in the outer shear ring groove remained unacceptably high.

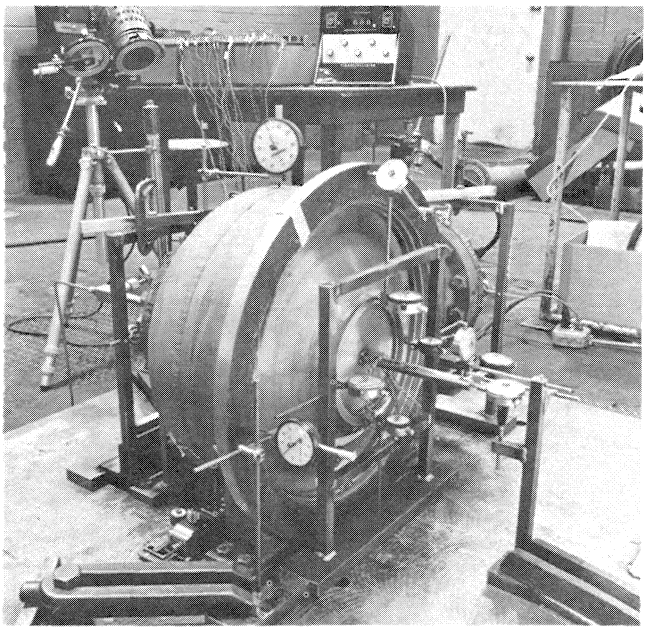

Figure 7. Model Test Set-Up.

The model casing was also subjected to simulated external piping loads applied to suction and discharge flanges. The set-up for these tests is shown in Figure 8.

At 1300 PSIG internal pressure, these external piping loads caused an additional .010″ axial deflection at the center of the main cover and a general pivot of the upper side of the casing opposite the discharge nozzle. The same loads applied at 1600 PSIG internal pressure, pivoted the casing less, and caused lower additive stresses in the discharge nozzle-to-flange weld-joint because of the increased shell stiffness. At neither pressure level did these simulated, high external piping loads seriously aggravate the previously observed stress levels.

The test results of this latest configuration, together with a new Finite Element Stress Analysis model, were used as the basis for a complete cover redesign. The change incorporated a significantly axially deeper and heavier configuration. The outer casing flange was also revised to further limit deflection. This redesign finally reduced cover stresses and deflections appreciably. Locally high stresses in the casing shear ring groove remained a problem, however, until back-up rings were wedged-in between shear rings and cover or bearing housing. These back-up rings reduced the tendency to shear ring tipping, or rolling about the loaded face.

In summary, the model tests helped to define a casing and cover design suitable for working pressures up to 1800 PSIG. The need for a high-strength material was confirmed. The intersection of discharge nozzle and casing was the only marginal area not subjected to several increasingly successful revisions. It was felt this area could be handled by analytical approaches and, therefore, the proof of the planned revision of this area, plus the confirmation of the acceptability of the stress levels in all critical areas, was left to the pressure tests on the full-size prototype.

Full-Size Prototype Tests

Following the conclusion of the model tests early in 1974 and a final analysis of the results, the casing and cover underwent a thorough redesign. This effort was primarily necessitated by the change in casing production methods from a fully

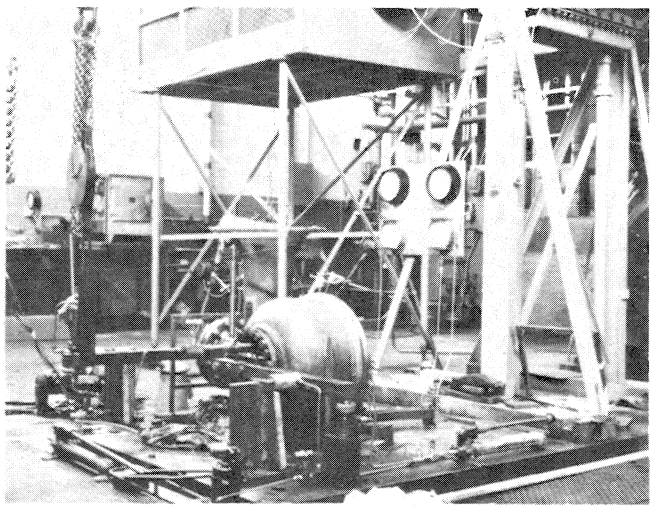

Figure 8. Model Casing Under Simulated External Piping Loads.

welded fabrication, using high-strength HY-80 plate, to an integral casting made from ASTM A-296 GR. CA-6NM. As previously mentioned, this change was made in response to increasing material procurement problems and a drastic cost escalation.

The full-size prototype casing became available for stress evaluation late in 1975. It was assembled and instrumented, closely paralleling all gauge and dial positions used on the model casing, to permit direct comparisons of results. A cover-end view of the fully assembled and instrumented prototype is shown on Figure 9.

The figure also shows the segmented inner and outer shear and wedge rings. A quarter-view of the main piping connections of the fully assembled and instrumented prototype is shown in Figure 10.

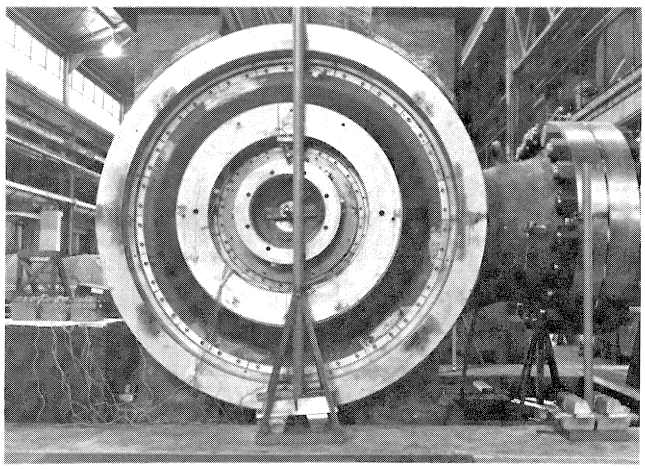

Figure 9. Full-Size Prototype on Hydrostatic Test, Cover-End View.

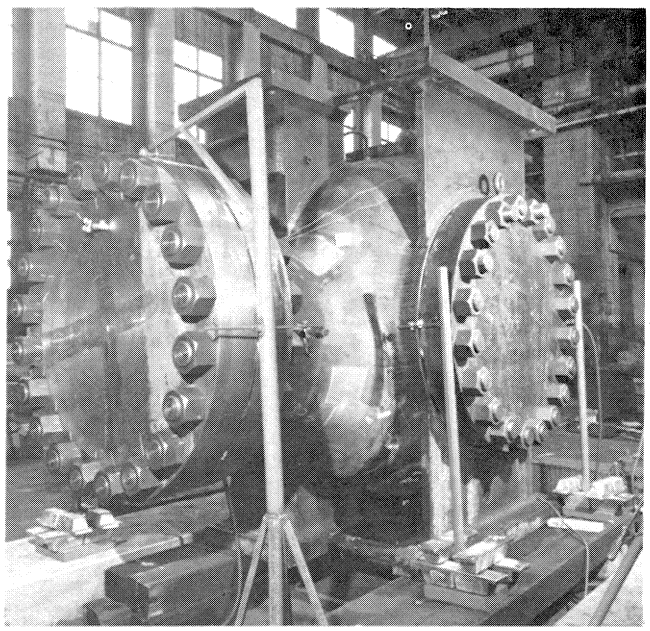

Figure 10. Full-Size Prototype on Hydrostatic Test, View of Main Pipe Connections.

Some of the areas covered by photo-elastic coating and backed-up by additional strain gauges are also visible. In spite of their massiveness (7″ thick), the blind flanges initially presented significant sealing problems caused, primarily, by the magnitude of their deflections under the maximum hydrostatic pressure of 2700 PSIG. These difficulties were overcome through the use of improved gasketing and nut torquing techniques. The complete redesign of this seal finally eliminated the problem entirely.

The Finite Element Stress Analysis technique, employed as a main design tool in all phases of this casing development, represents a major advance in the field of stress calculations. It permits the prediction of average, or highly localized skin stresses, of very complex configurations with sufficient accuracy for most design purposes. Its use requires access to a fair size computer and a lot of patience on the part of the designer. (The preparation of the initial input for large, complex shapes often consumes several days of rather exacting work plus experience in the selection of suitable element sizes to obtain satisfactory results). The computer drawn element plot of the final RFA36 compressor casing is shown in Figure 11 in unpressurized condition.

The deformed element plot of this same casing under 2700 PSIG hydrostatic pressure is shown on Figure 12 (deformations 35X magnified).

The hydrostatic testing of the full-size model was preceded by a detailed dimensional inspection of casing and cover. This was followed by the actual hydrostatic tests, during which the casing pressure was gradually raised to 1800 and finally to 2700 PSIG, while stresses, deflections, and photo-elastic observations were carefully recorded at each step. Frequent excursions back to 0 PSIG were made to detect points of yielding and to monitor potentially critical strain levels. Hydrostatic pressurization to 2700 PSIG was subsequently repeated to confirm the absence of further yielding. Following these excursions, additional observations were made during several repressurizations to 1800 PSIG to check and confirm stress and deflection levels recorded earlier. Subsequently, the casing was disassembled and subjected to a detailed dimensional inspection, followed by a close dye-penetrant check of the shear ring grooves. The casing was then reassembled and rehydrotested. A gas test (Nitrogen) followed. The casing was pressurized to 1800 PSIG, where it was held for one hour with disconnected pumps, and no pressure or gas losses occurred.

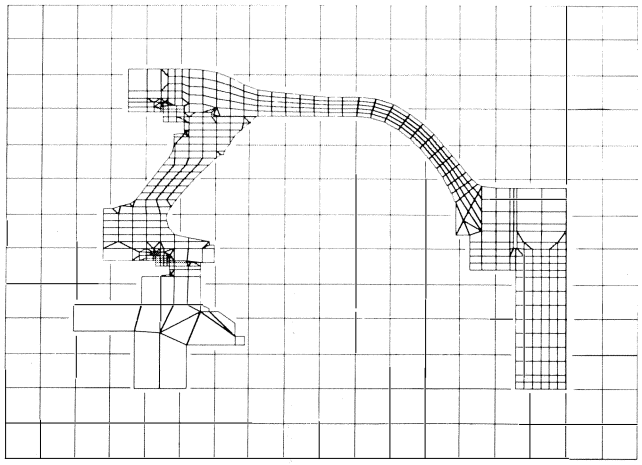

Figure 11. Finite Element Stress Analysis, Element Plot.

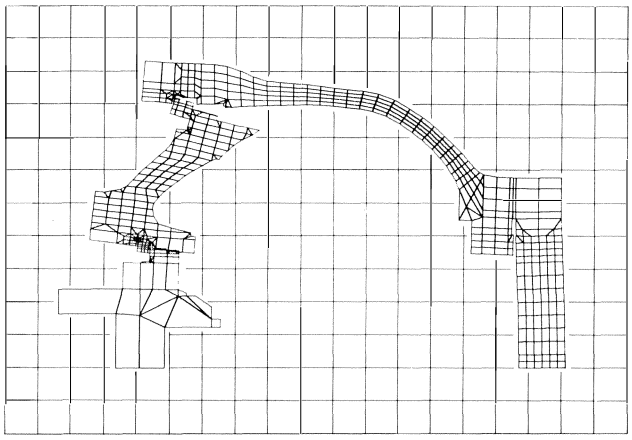

Figure 12. Finite Element Stress Analysis, Deformed Element Plot at 2700 PSIG.

Final dimensional and dye-check inspections concluded the static pressure test phase.

Following is a summary of the results of this series of static pressure tests:

1. Photo-elastic coating patterns backed-up by strain gauges reflected a flat, low-stress level response (free of the earlier stress concentrations) up to 2700 PSIG confirming the successful redesign of this intersection of casing and discharge nozzle. Stresses remained well below one color fringe (40.5 KSI for this material).
2. Cover and bearing housing seals (o-ring) showed significant evidence of flattening after exposure to 2700 PSIG, but caused no leakage problems, on water or gas. No visible deformations were observed up to 1800 PSIG.
3. Permanent deformations, typical for well-stressed, pressure vessels, remained within acceptable limits and neither required remachining nor could increases be observed during subsequent excursions to previously reached pressure levels.
4. Elastic deflections, reaching a maximum of .138″ at 1800 PSIG at the outer face of the bearing housing, can be accommodated without problems. Significant data, valuable in future field installation work, was obtained.
5. Maximum stress levels observed at 2700 PSIG was 101.4 KSI measured in the outer shear ring groove fillet. The peak stress observed at 1800 PSIG in the same location was 81.0 KSI during initial pressurization up to 2700 PSIG. Observations made during subsequent pressure cycles confirmed the lower values expected during field operation (72.3 KSI max.) They are lower because of the hysteresis effect. Consequently, the maximum operating stress will remain comfortably below the yielding level (.2% offset) even in this area.
6. The magnitude of the peak working stress level in the outer shear ring groove at 1800 PSIG (72.3 KSI) exceeds the proportional limit (.02% offset). Consequently, low cycle fatigue life was investigated. The calculations show LCF to be one million pressure cycles at 90,000 PSI load stress for this material.

Comparison of Experimental and Analytical Stresses and Deflections

A brief comparison of stresses and deflections calculated and observed on model and full-size casings will help to summarize these efforts. Figure 13 describes the positioning of the various stress and deflection measurement points; generally each symbol identifies a typical position of an instrument. However, identical instruments monitoring identical areas in different clock positions are not shown to avoid unnecessarily complicating the figure.

The following table compares stresses and deflections observed and calculated in the various areas:

COMPARISON OF MODEL AND FULL-SIZE PROTOTYPE TEST RESULTS WITH FINITE ELEMENT ANALYSIS PREDICTIONS AT 2700 PSIG

LOCATION	ELASTIC STRESS/DEFLECTION MODEL	FEA	FULL-SIZE	ERROR MODEL	FEA
G	.212″	.180 ″	.198 ″	+ 7%	− 9%
P	.176″	.186 ″	.1955″	− 10%	− 5%
A	.176″	.173 ″	.168 ″	+ 5%	+ 3%
AA	.071″	.085 ″	.045 ″	+ 58%	+89%
K(INNER)	—	.0071″	.0218″	—	−67%
K(OUTER)	—	.0072″	.0380″	—	−81%
H	.038″	.0167″	.0170″	+124%	− 2%
Z	151.0 KSI	104.0 KSI	101.4 KSI	+ 49%	+ 3%
Y	28.0 KSI	47.3 KSI	69.9 KSI	− 60%	−32%
TT	− 22.5 KSI	− 27.8 KSI	− 55.5 KSI	− 59%	−50%
W	− 51.0 KSI	−102.9 KSI	− 68.6 KSI	− 26%	+50%
M	—	13.0 KSI	14.8 KSI	—	−12%

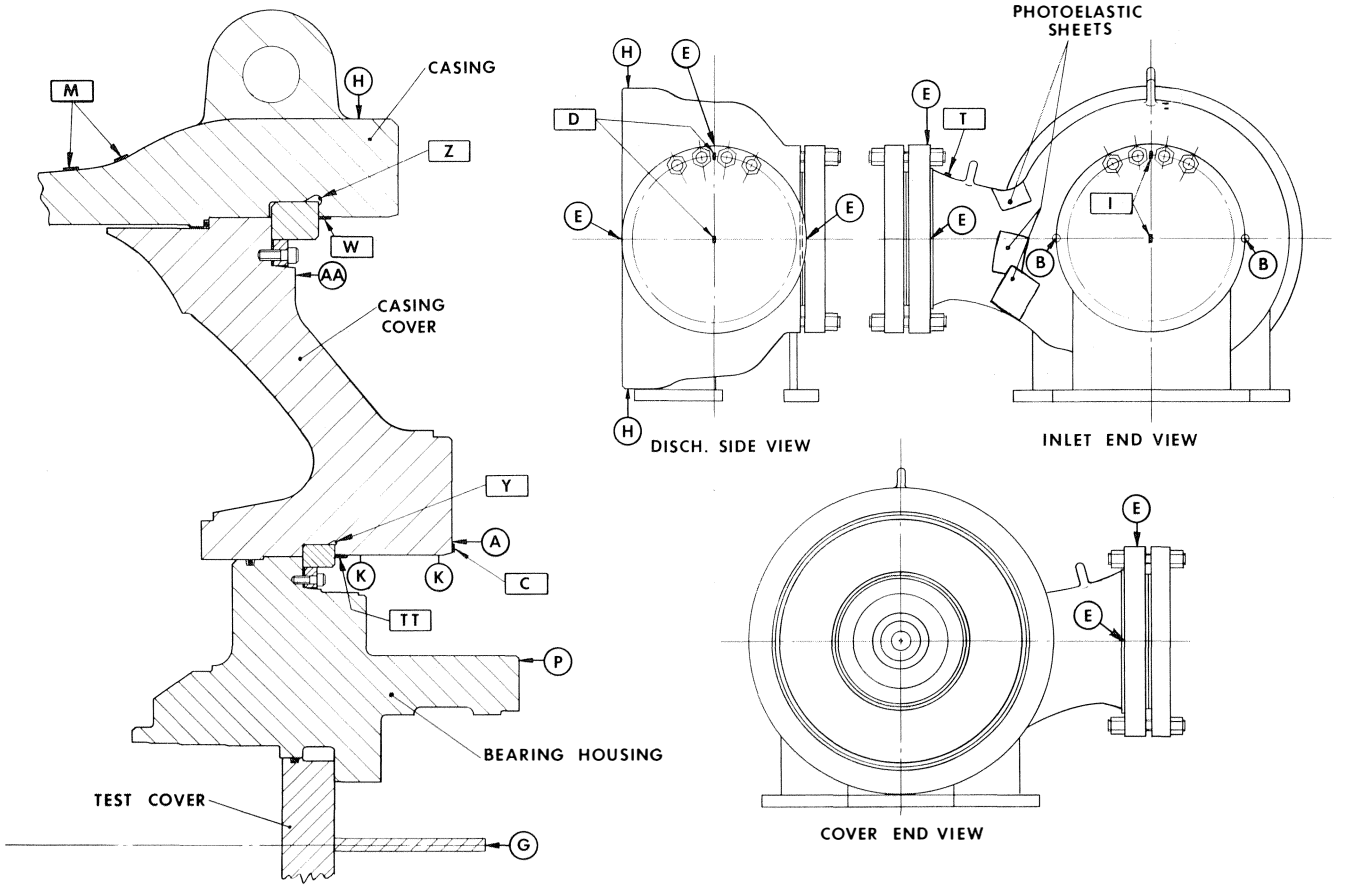

Figure 13. Casing Strain and Deflection Instrumentation.

The previous tabulated values represent the peak stress and deflection readings observed where multiple gauges in different clock positions were used.

The tabular comparison shows, with a few explainable exceptions, generally good correlation (±15%) between the experimental results observed on the full-size prototype and the Finite Element Stress Analysis (FEA). The three not readily explainable exceptions are the deflections in the cover bore (K (Inner) and K (Outer)) and the stress in the cover shear ring groove fillet (Y). In all three instances, actual values were underestimated. However, the 50% low FEA prediction just outside the inner shear ring (TT) is probably largely due to the difference between element size and gauge length (.3125″ vs. .125″, respectively) in an area with a relatively steep stress gradient. The 50% high FEA prediction next to the outer shear ring (W), in spite of another element size/gauge length difference, is probably due to the fact that the FEA neglects yielding, which conceivably would have relieved these stresses considerably. Finally, the 89% high FEA prediction on the outer cover face near the O.D. (AA) is attributed to the absence of wedge-up sections in the FEA model, due to the lack of a suitable modeling method.

The tabular comparison also shows generally unsatisfactory correlation between the ¼ scale model and the FEA results, except in the area of cover deflection (±10%). The generally lower model stresses were probably due to averaging effects over the strain gauge lengths. The model should have had active strain gauge lengths equal to ¼ of the gauge length used on the full-size prototype; however, they were generally about ½. The higher model stresses in the outer shear ring groove fillet (Z) is attributed to the absence of wedge-ring sections in the model. In addition, it should be remembered that the casing was redesigned to be cast following the model tests, a fact that limits direct comparisons.

These extensive casing development efforts confirm the success of this casing design and provide most valuable experience in the use and interpretation of the Finite Element Stress Analysis.

AERODYNAMIC PERFORMANCE EVALUATION

Since the achievement of aerodynamic efficiencies of 85 to 87% (isentropic) represented the primary objective of this pipeline booster development, considerable effort was put into the planning, preparation, conduct and analysis of these tests and their results.

Test Arrangement

The requirement to approximate a rather high Reynold's number under typical field conditions (2.12×10^8 at compressor inlet), the desire to obtain precise performance data, the need for closely controlled relative pressure measurements, and the known effects of small quantities of ingested dirt on efficiency all combined to dictate a closed loop test vehicle. Loop pipe size and pressure level were chosen to provide the best balance between adequate representation of the Reynolds number and capability to reach up to 35,000 ACFM. These considerations led to the design and construction of the medium-pressure test facility shown in Figure 14.

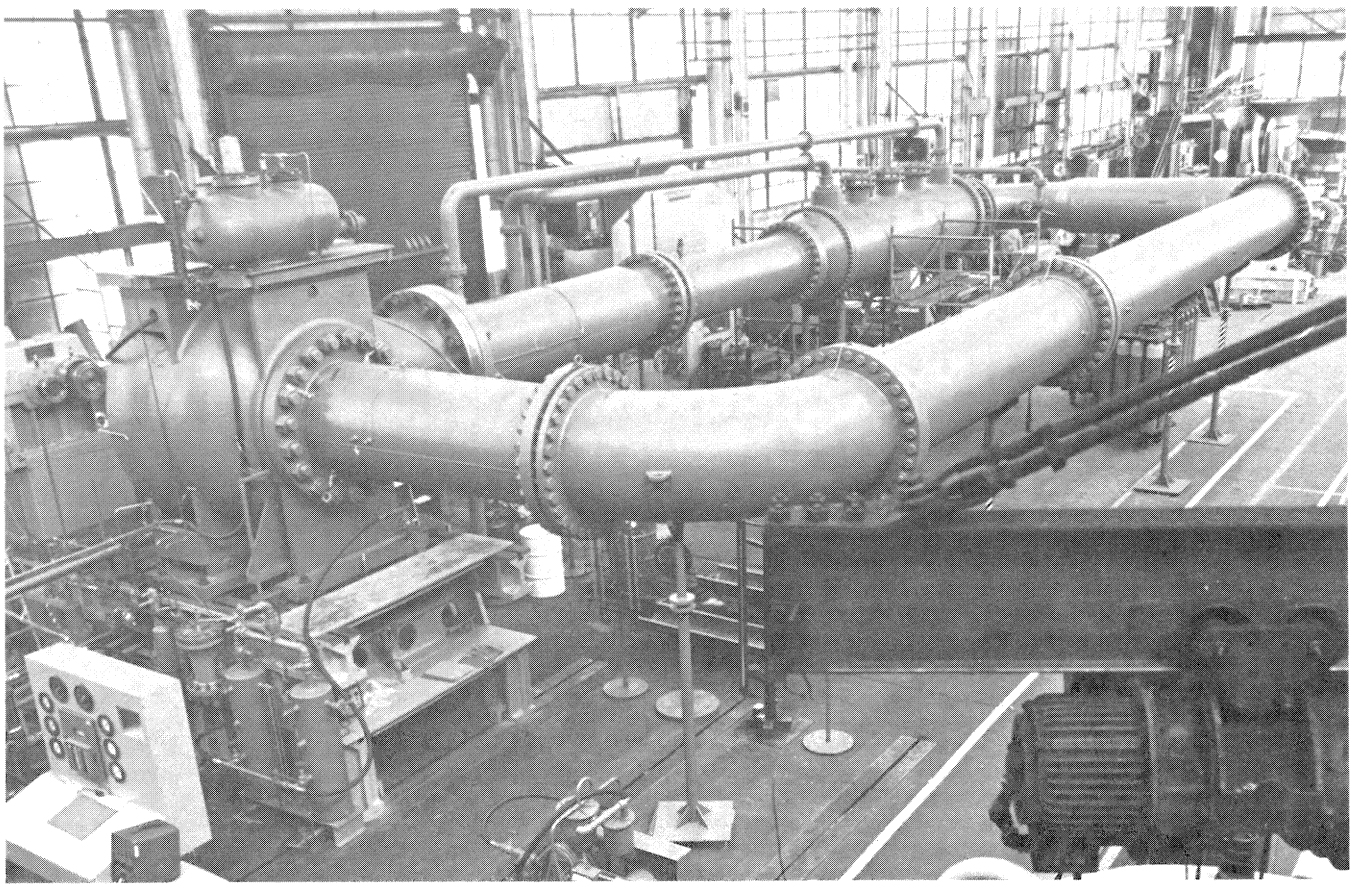

Figure 14. Performance Test Facility.

This test facility was designed to permit the evaluation of the compressor performance on nitrogen (selected for safety reasons) at pressure levels of up to 350 PSIG (necessary to raise test N_{RE} — number to 10% of the field N_{RE} — number). Its driver, a jet-engine powered gas turbine, is capable of 10,500 SHP and 5,200 RPM. Most of the aerodynamic performance testing power requirements were around 6000 - 6500 SHP with peak demands of up to 7300 SHP. As Figure 14 reflects, the effort to minimize pressure drops in the loop, resulted in the use of large pipe sizes: 36″ diameter pipe was used for all sections of the loop except for a short run of 30″ diameter pipe leading to a 30″ diameter heat exchanger. The selection of the pipe diameter defined the minimum loop size required to provide satisfactory aerodynamic test conditions (flow control) and meet applicable test codes (ASME PTC 10 and supplements). The use of the 45 foot long, straight flow measuring section shown on Figure 14 is only the most apparent of the consequences of these considerations.

The large size of this test loop presented several major problems in the planning stages of which only one required a deviation from the ideal set-up. Due to space limitations, the ideal length of straight pipe leading to the compressor inlet flange of 10 pipe diameters could not be accommodated. To confirm the negligible effect of this deviation on inlet pressure measurement, the pressure distribution in the intake pipe was measured and analyzed. These results are reviewed as part of the aerodynamic performance evaluation.

For the positioning of all loop instrumentation, the guidelines detailed in the Power Test Code were strictly adhered to.

The following summary describes the instrumentation used for the acquisition of all aerodynamic data:

— *Flow measurement* was accomplished with a standard 15″ diameter long-radius nozzle.

— All *loop temperatures* were measured with exposed resistance temperature detectors connected to a digital temperature indicator. This complete system was calibrated with a high-precision thermometer to read within ± 0.10°F. Since the gas velocities at the measurement points in the loop remained below 125 ft/sec throughout all tests, only static temperatures were measured and the velocity effects neglected.

— All *loop pressure levels* were read on a temperature-compensated 12″ diameter Bourdon-tube type pressure gauge calibrated to read within 1.0 PSI. Only static loop pressures were measured, as no calculated velocity pressure exceeded 5% of the overall static pressure rise across the compressor even under maximum flow conditions. All velocity pressures in the loop were calculated to obtain the required stagnation (total) pressures.

— All *differential pressures* including the overall compressor pressure rise were measured with suitably filled high pressure liquid manometers.

In addition to the loop data, a large number of compressor internal data points were monitored throughout the entire aerodynamic test to supply the data necessary to analyze the performance of different areas in the aerodynamic assembly.

These results were used as a basis for judgements on feasibility and extent of possible further performance improvements.

To minimize the flow disturbance effects of this internal instrumentation, only static measurements were taken. These consisted primarily of pressure measurements supplemented by temperature measurements in a few locations. The positioning of the internal static pressure probes is shown in Figure 15.

All these internal pressure levels, appropriately referenced to inlet or discharge pressures, were monitored as differential pressures on large banks of liquid-filled, single-leg manometers. To assure simultaneous readings, these manometer banks were photographed at suitable time-intervals. To supplement these static pressure readings, the pressure fluctuations in the vaneless diffuser were monitored with a transducer and recorded on a visicorder oscillograph.

Method of Analysis of Test Results

Although designed for natural gas compression, this pipeline booster was tested aerodynamically almost exclusively on nitrogen. Safety considerations and restrictions made the use of natural gas impractical. Consequently, in preparation for the thermodynamic performance data, several different sources of nitrogen data were thoroughly reviewed. Detailed comparisons of data published by Din, the National Bureau of Standards (NBS), Southwest Research Institute and computerized Benedict/Webb/Rubin (BWR) results were made. Significant differences affecting isentropic efficiencies by up to ± 0.5 percentage points were found. The review confirmed close agreement between the NBS tables and one BWR approach over the pressure and temperature ranges expected for these tests. As a result, the BWR analysis matching the NBS tables was used as the basis for the reduction of all aerodynamic test data.

The results obtained during each performance test run were subjected to the following computerized calculation procedure:

1) Averaging of all (usually five) readings for each set point
2) Correction for instrument calibration
3) Conversion of all static to stagnation pressures (ASME PTC 10)
4) Calculation of actual inlet flows, isentropic heads and gross efficiencies from calculated entropies based on BWR/NBS analysis
5) Efficiency correction for radiation loss using ambient and casing temperatures (ASME PTC 10)
6) Conversion of results into dimensionless parameters for actual inlet flow (ϕ) and head (ψ)

It should be noted that accuracy and consistency in data acquisition and analysis is critical at these performance levels, as an error of 0.10°F on suction and discharge temperatures can add up to a 0.2°F error in temperature difference which will change the efficiency by about 0.5 percentage points.

The following definitions are used for the dimensionless coefficients:

$$\phi_s = \frac{3.056 \cdot Q_s}{u_2 \cdot D_2{}^2} = \text{Inlet flow coefficient}$$

$$\psi_{is} = \frac{H_{is} \cdot g}{u_2{}^2} = \text{Isentropic pressure (head) coefficient}$$

Where: Q_s = Inlet flow (ACFM)
D_2 = Impeller (outer) diameter (inch)
u_2 = Impeller tip speed (ft/s)
H_{is} = Isentropic head (ft. lbs/lb)

This completes the calculation of the actual test results. From the individually calculated test points, a mean efficiency curve was calculated through a computerized interpolation method based on the head-flow curve and linear relationship between head/efficiency and flow.

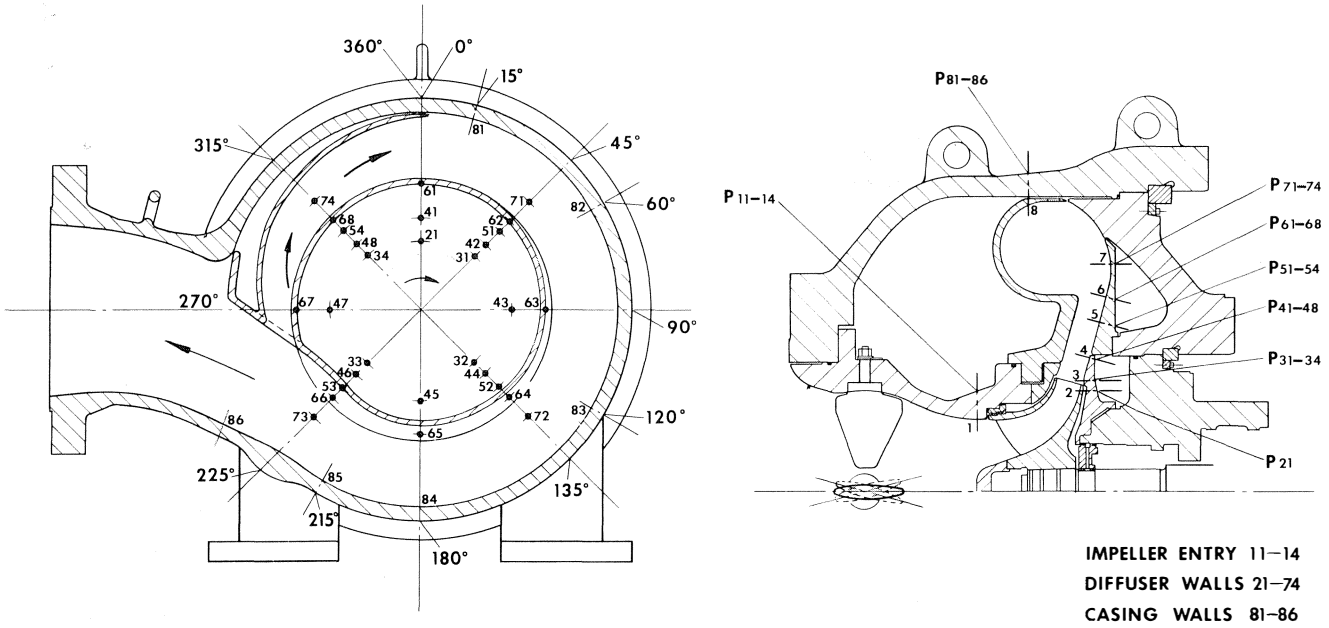

Figure 15. Position of Internal Static Pressure Probes.

Performance Test Results

Prior to the discussion of the actual aerodynamic performance test results, the selection of the test speed should be reviewed briefly:

The aerodynamic design of the prototype was based on the following operating conditions:

Inlet volume flow	= 22,000 ACFM
Suction temperature	= +2°F
Suction-Discharge pressure	= 1380 - 1691 PSIA
Design speed	= 4760 RPM

The calculations made for the selection of a test speed illustrate an interestingly large discrepancy between different scale speeds:

Condition	Operating Speed	Maximum Mach-No.	Volume-Reduction
Field	4760	.481	.9225
Test	4220	.349	.9225
Test	5680	.481	.8617
Test	5000	.421	.8855

These figures confirm that testing at the Mach-number scale speed of 5680 RPM would have resulted in an unacceptably poor match in volume reduction. This unusually large discrepancy between the two scale speeds necessary to match volume reduction and Mach-number under field conditions is attributable to the extremely low compressibilities (0.60 - 0.64) encountered at the low temperatures and relatively high pressures typical of gas operating conditions realized in the arctic.

The overall aerodynamic performance of the prototype is shown in Figure 16.

The wide operating characteristic permitting continuous stable operation from 14,500 to over 38,000 ACFM at 5000 RPM, is generally typical of a properly designed, single-stage pipeline booster. In this case, it is enhanced by the very modestly loaded inducer-type impeller designed to meet the specific operating conditions selected for the aerodynamic assembly used in the prototype. In addition, the efficiency goal of 85 to 87% was reached over a flow range exceeding 8800 ACFM. It should be noted that any special efforts which could improve aerodynamic efficiency were consciously avoided — all compressor components were machined to the same detail drawings to which future production units will be built. No special fitting work to achieve smaller tolerances or polishing efforts to improve surface finishes was permitted. No significant assembly problems were encountered. Only minor adjustments, primarily involving the use of the special assembly tooling, were necessary.

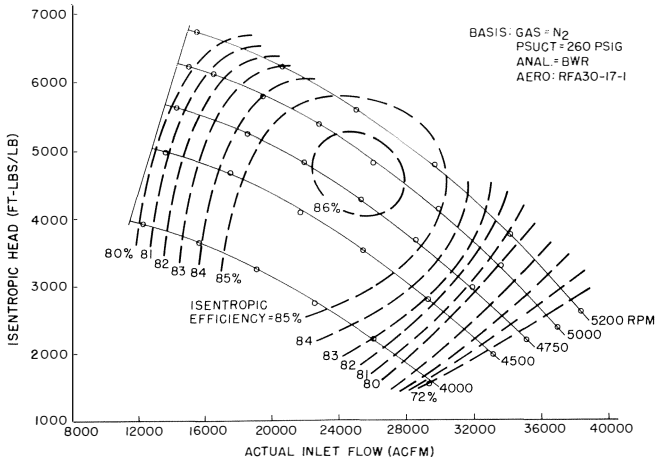

Figure 16. Compressor Aerodynamic Performance Map.

The results of the next tests, shown on Figure 17, clearly illustrate the pressure level effects on performance.

Generally, little influence on head, but significant effect on efficiency (over 1.0 percentage point) are experienced. Both performance runs compared were made on a closed loop: the low pressure tests were originally planned to be made on an open loop, but out of concerns for fouling and for generally poor control over suction conditions resulting in inconsistent data and significant delays in project progress, a low pressure closed loop run was substituted. The Reynolds-numbers at the compressor inlet were under field operating conditions around $2 \cdot 10^8$, under 260 PSIG test conditions around $2 \cdot 10^7$ and under 1 PSIG test conditions around $1 \cdot 10^6$. These results demonstrate the necessity for aerodynamic performance testing at sufficient pressure levels to eliminate N_{RE} and heat transfer effects, particularly in cases where a highly accurate efficiency determination is of prime importance. It would appear that the code-suggested guidelines on N_{RE} simulation in aerodynamic performance tests are adequate (N_{RE} test = (0.10 - 2.0) $\cdot N_{REfield}$).

The selection of a test gas was also confirmed to be of considerable importance. Data taken during runs made with carbon dioxide using the same test rig and instrumentation, correlated well with results generated with nitrogen on a head-flow basis, but led to unbelievably optimistic efficiencies (well over 90%). A review of several data sources for carbon dioxide

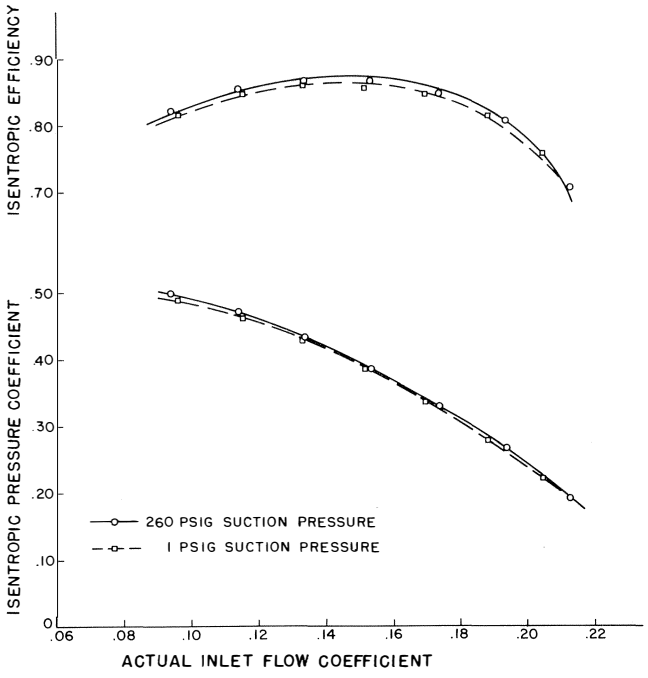

Figure 17. Effect of Loop Pressure on Aerodynamic Performance.

did not result in the discovery of one highly consistent and reliable source for property values, as a similar review of nitrogen source data had found earlier. The conduct of the actual test work with CO_2 proved to be a far more delicate and time-consuming task, compared to similar nitrogen runs, and consequently led to less consistent results even on a head-flow basis. This experience underscored the need for highly reliable thermodynamic data on the test gas (at least within the intended operating range).

In the performance tests, the effects of open and closed volutes on overall compressor performance were investigated (reference Figure 18).

To permit a direct comparison without introducing additional variables, a volute extension was designed to close the open volute used in the aerodynamic assembly in the prototype. This is shown in Figure 19.

Analytical studies, past and present, invariably support the exclusive use of closed volutes because they prevent flow recirculation almost completely. Our own tests show the closed volute to have a very slight peak efficiency advantage (around 0.30 efficiency points), but also to have a somewhat steeper efficiency curve. Effects on head development are clearly negligible. The analysis of the compressor internal static pressure distribution, closely monitored under all test conditions, confirms the disturbing effect of the volute cutwater on static pressure distribution. This basic effect is observed on both open and closed volutes and is primarily evident at lower flows. A closer examination, however, confirms the open volute to cause a stronger pressure disturbance, extending to somewhat higher flows than with the closed volute. In fact, based on measured data, the effect of the improved pressure distribution with the closed volute on overall compressor performance was disappointingly small.

To dispel concerns over the magnitude of the effect of the reduced length of straight pipe between the final long-radius

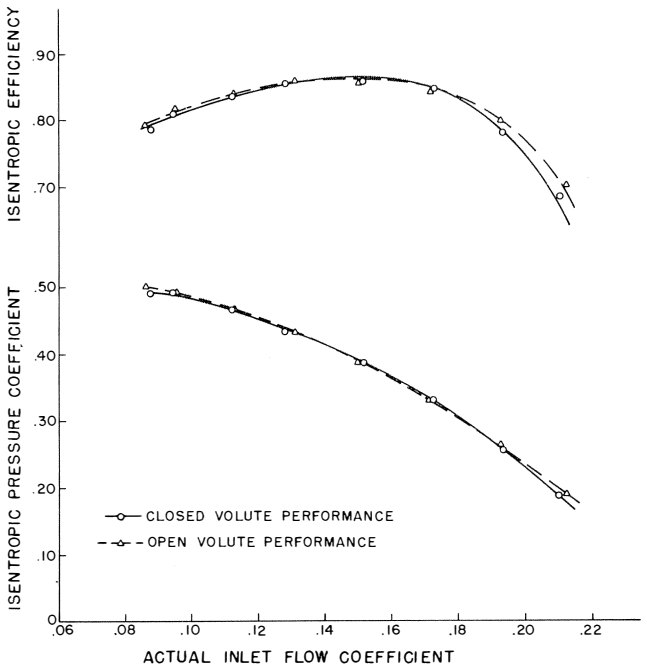

Figure 18. Effect of Volute Design on Aerodynamic Performance.

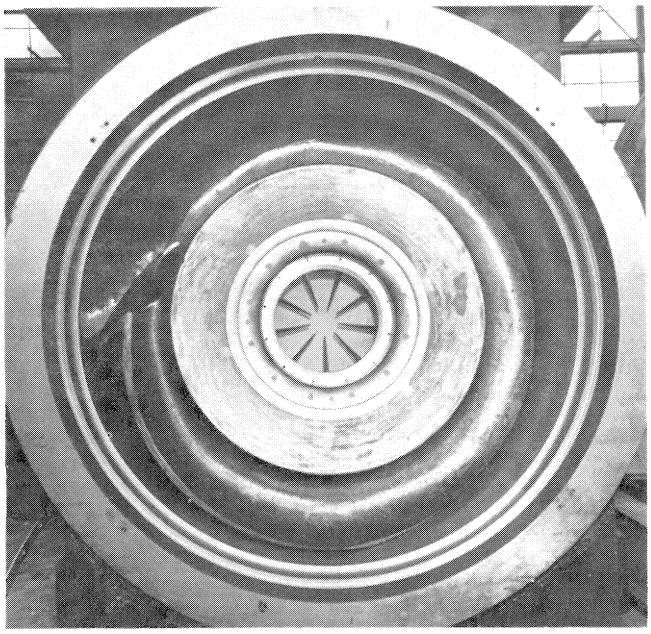

Figure 19. Discharge Volute with Insert.

elbow and the compressor inlet, a series of pressure traverses at two different positions in this intake pipe (at one and two pipe diameters (72″ and 36″) upstream of the compressor flange) were made. The results of these efforts are shown in Figure 20.

These traverses were made at a static pressure level of 135 PSIG on nitrogen. As expected, the effects of the 90 degree elbow (in horizontal plane) are clearly evident and strongly accentuated at higher flows. To reduce congestion of Figure 20, the symmetric pressure distribution in both vertical planes is only shown to the center of the pipe. Since the calculated mean velocity pressures were considered in the data reduction process, only the effect of differences between mean and actual velocity pressures needed to be considered. An evaluation of the velocity pressure differences shows, however, that the effect of this pressure distortion is well within the measuring

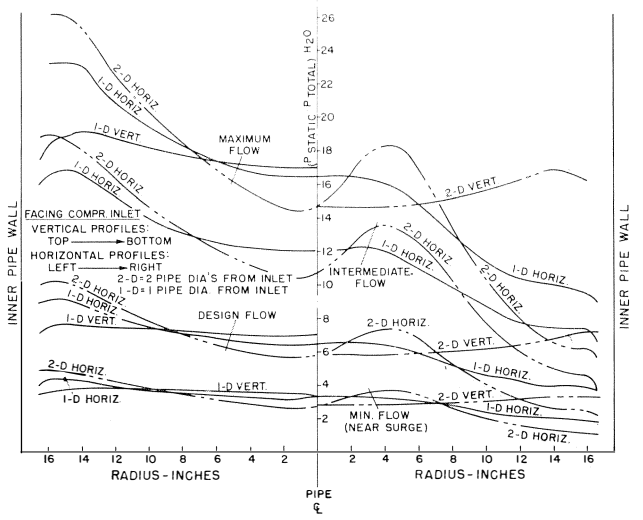

Figure 20. Pressure Distribution in Intake Pipe.

accuracy at all, but perhaps the maximum flows. In spite of this fact, the use of a more effective flow-straightener is planned for all future tests, which in combination with additional pressure traverses, will dispel any remaining concerns.

This completes the review of the major results obtained during the aerodynamic performance test phase. These aero tests extended over more than 150 hours of actual test time, many of these spent in confirming the repeatability and consistency of previous tests. Each of these checks proved to be highly successful. Throughout these tests the absence of loop contamination (dirt, oil) and pressure loss through leaks, was maintained. Because of the highly detrimental effects of oil contamination on efficiency, the prototype was subjected to very careful examinations of all its aerodynamic flow surfaces during each of the numerous internal booster inspections. Not even a single trace of oil could be found during any of these examinations, an indication of the effectiveness of the buffer gas arrangement and generally careful operation.

MECHANICAL EVALUATION

The mechanical evaluation of this new booster design presented no problems. The majority of the programs were generally undertaken to either prove the adequacy of the design or just gather data useful in later installation work.

Seal Performance

To establish the seal performance under representative operating conditions, the aerodynamic assembly was removed from the compressor and replaced with a small housing designed to permit the application of higher pressures to the shaft-end. This housing was then pressurized with helium to pressures of up to 1400 PSIG, a limit imposed by the seal oil system used. This arrangement permitted the seals to be tested with results as shown on Figure 21.

The effect of shaft speed and gas pressure on outer seal oil flow rate is typical and expected for this type of unit. Beyond 1400 PSIG only static oil flows were measured.

Thrust Bearing Performance

Since a directed-lubrication thrust bearing is used in this booster (a relatively new thrust-bearing design), its performance under high thrust loads at start-up and at speed, was of considerable interest. The thrust bearing performance under load, shown in Figure 22, presented neither problems nor surprises.

The moderate peak pad temperatures confirmed adequate reserve capacity. The pressure limitation listed in the seal performance discussion restricted the loading of the thrust bearing to 40,000 lb. at different speeds. Following these running tests, a number of pressurized starts were made to confirm the suitability of the directed-lubricated thrust bearing for this application. Again, no problems were found.

Breakaway Tests

The mechanical testing of the RFA36 was concluded with a series of breakaway tests. These were made to obtain data for later use in the selection of suitable drivers.

CONCLUSIONS

A review of this design development enables the following conclusions to be made:

1) Aerodynamic performance with isentropic efficiencies of 85 - 87% can be achieved if sufficient care is taken in the design. In particular, the inlet configuration, flow area and surface control, and precision in impeller production are important.
2) Closed volutes offer only slightly peak efficiency improvements over open volutes despite their obvious analytical superiority.
3) Matching of field Reynolds numbers within the code-specified limits of 10-200% during shop performance

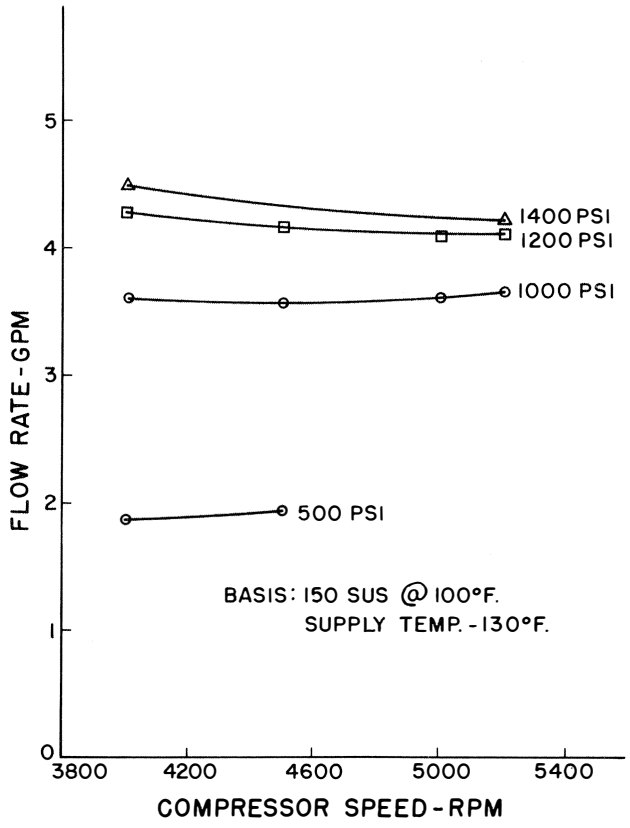

Figure 21. Outer Seal Performance.

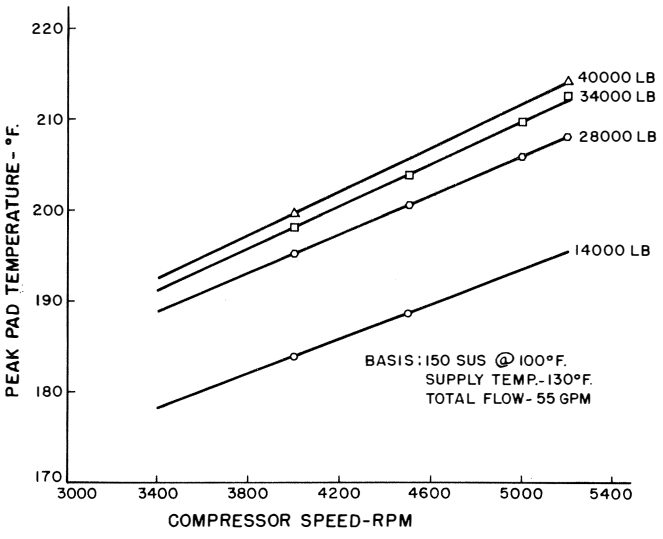

Figure 22. Thrust Bearing Performance.

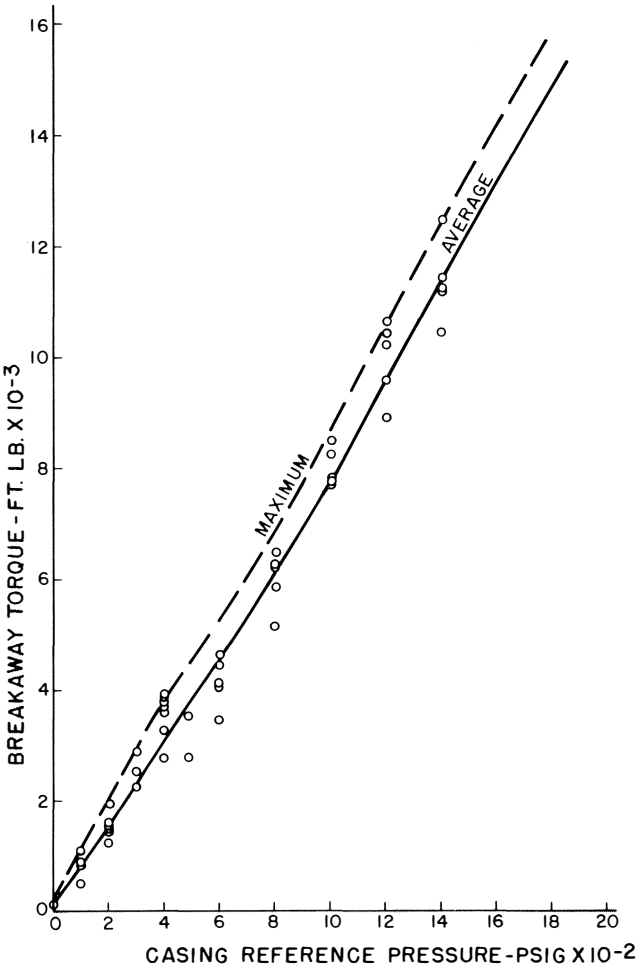

Figure 23. Breakaway Torque.

tests is essential to achieve efficiencies expected under field operating conditions. Reynolds number effects on head are insignificant.

4) With an axial inlet, the use of an effective flow straightener following an elbow is recommended, particularly where code-required straight lengths of inlet pipe cannot be accommodated. Pressure traverses run downstream of the flow straightener may be used to confirm the magnitude of the remaining flow distortion.

5) The availability of highly reliable thermodynamic source data on the selected test gas is essential to precise aerodynamic performance testing.

6) The successful development of a large, high pressure casing is greatly accelerated through the judicious use of a Finite Element Stress Analysis model. The correlation between the results obtained from a well-designed element model and the full-size casing is excellent.

7) The ¼ size model contributed significantly to the definition of the final casing and cover configuration. It permitted the rapid implementation of the necessary major revisions at a minimum cost. Unsatisfactory correlation with FEA results were due to the proportion differences between the fabricated model, the cast prototype and its FEA simulation.

8) The conduct of a highly instrumented, full-size hydrostatic pressure test combined with a low-cycle fatigue analysis is essential to confirm the adequacy of large, high-pressure casings, particularly where shear ring retention is used.

9) The use of a shear ring closure necessitates a careful material selection and tight controls of the shear ring groove configuration.

10) The evaluation has shown that even with an axial inlet and a tangential discharge, external pipe forces and moments typically accepted on conventional pipeline boosters (opposed nozzles) can be accommodated.

11) The use of a positive arrangement to eliminate any possibility of introducing oil into the aerodynamic assembly is essential in the preservation of highest efficiencies in prolonged operation.

12) The beneficial performance of the relatively new type thrust bearing using directed-lubrication, for an over-hung compressor design with its traditionally high starting thrust loads, has been confirmed.

13) The experimental phase of this development program confirmed the satisfactory aerodynamic and mechanical performance of this new, high-flow centrifugal pipeline booster meeting all design expectations.